Talanta 85 (2011) 1105–1111

Contents lists available at ScienceDirect

Talanta

journal homepage: www.elsevier.com/locate/talanta

Humidity sensing properties of ZnO-based fibers by electrospinning

Nesrin Horzum[a], Didem Taşçıoglu[a], Salih Okur[b,*], Mustafa M. Demir[a,**]

[a] İzmir Institute of Technology, Faculty of Science, Department of Chemistry, 35430 İzmir, Turkey
[b] İzmir Institute of Technology, Faculty of Science, Department of Physics, 35430 İzmir, Turkey

ARTICLE INFO

Article history:
Received 31 January 2011
Received in revised form 9 May 2011
Accepted 17 May 2011
Available online 26 May 2011

Keywords:
Electrospinning
Zinc oxide
Humidity
Sensor
Calcination

ABSTRACT

Zinc oxide (ZnO) based fibers with a diameter of 80–100 nm were prepared by electrospinning. Polyvinyl alcohol (PVA) and zinc acetate dihydrate were dissolved in water and the polymer/salt solution was electrospun at 2.5 kV cm^{-1}. The resulting electrospun fibers were subjected to calcination at 500 °C for 2 h to obtain ZnO-based fibers. Humidity sensing properties of the fiber mats were investigated by quartz crystal microbalance (QCM) method and electrical measurements. The adsorption kinetics under constant relative humidity (RH) between 10% and 90% were explained using Langmuir adsorption model. Results of the measurements showed that ZnO-based fibers were found to be promising candidate for humidity sensing applications at room temperature.

1. Introduction

Sensing and controlling humidity are particularly significant for both human life and various industrial fields. The major domestic applications of humidity sensors have been the humidity control in heating, ventilating and air conditioning (HVAC) systems, food packaging, greenhouse agriculture, the production of electronic devices, automotive industries, and in meteorology stations. In respond to the strong demand for automatic control systems, reliable, cheap, sensitive humidity sensors operated at ambient temperatures are of critical importance [1].

Sensing devices based on metal oxide semiconductors with nanostructures have perfect chemical reactive surfaces that have water adsorbing and desorbing properties, thermal stabilities, and mechanical durability [2–5]. The considerable attention has been focused on the studies of one dimensional (1D) nanostructured metal oxides, *i.e.* nanorods [2,6], nanowires [2,3], nanoparticles [7], nanotetrapods [8], or nanofibers [9–14], and their influence on the humidity sensing performance. Many available techniques such as carbothermal reduction synthesis [15], chemical vapor deposition (CVD) [16], electrospinning [12], hydrothermal synthesis [17], vapor–liquid–solid (VLS) [18], conventional precipitation [19,20] have been attempted to obtain nanostructures. Among them, electrospinning provides a convenient and facile route for the fabrication of fibrous materials possessing high surface area to volume ratio, uniform diameters and variety of composition. It is a robust method for the production of not only polymeric [21], but also composite [22,23] and ceramic fibers [24] with diameters ranging from several nanometers to few micrometers. Moreover, chemistry tool box of electrospinning process is very wide. To date, >200 polymer/solvent systems have been processed by this method. In addition, electrospun mats have superior mechanical property compared to the others in terms of integrity. They provide an integral body even if they are subjected to calcination process.

Zinc oxide, which is a wide band gap (3.37 eV) semiconductor with large exciton binding energy (60 meV) [23–25] is an ideal candidate on the production of sensors [26,27]. Previously, Qiu and Yang [8] presented that ZnO nanotetrapod film exhibited much higher sensitivity to humidity than ZnO nanoparticles and investigated the response and recovery time as 36 and 17 s, respectively. Hu et al. [28] evaluated response (50 s) and recovery (6 s) behavior of ZnO colloidal nanocrystal clusters. An efficient humidity sensor based on ZnO nanorods was reported by Qi and co-workers [6]. LiCl-doped ZnO nanofiber humidity sensor was studied by Wang et al. [11]. The best result is obtained for 1.2 wt% LiCl-doped sample, which exhibits high humidity sensitivity, rapid response (3 s)–recovery (6 s) and good reproducibility. Qi et al. [10] suggested 5.7 wt% KCl-doped ZnO nanofibers as humidity sensor with super-rapid response (2 s) and recovery (1 s). Zhang et al. [9] recently showed a contribution on Na^+-doped ZnO nanofiber membrane for humidity sensor underlying the effect of NaCl doping as 4.6 wt% and reported the response (3 s) and recovery (6 s) behavior. However,

* Corresponding author. Tel.: +90 232 7507706; fax: +90 232 7507707.
** Corresponding author. Tel.: +90 232 7507511; fax: +90 232 7507509.
E-mail addresses: salihokur@iyte.edu.tr (S. Okur), mdemir@iyte.edu.tr (M.M. Demir).

0039-9140/$ – see front matter © 2011 Elsevier B.V. All rights reserved.
doi:10.1016/j.talanta.2011.05.031

the humidity sensing properties and adsorption–desorption kinetics of pure ZnO nanofibers have not been reported. In the present study, we demonstrate a simple and effective route for the synthesis of ZnO nanofibers with rapid response (0.5 s) and recovery (1.5 s) to humidity. The adsorption kinetics of the fiber sensor was investigated by QCM technique which is one of a wide branch of surface acoustic wave (SAW) techniques [14]. The change in resonance frequency of QCM was observed with increasing relative humidity up to 90%. The adsorption kinetic parameters were examined using Langmuir model.

2. Experimental details

2.1. Preparation and characterization of ZnO nanofibers

In a typical procedure, a sample of 2.5 g of zinc acetate dihydrate ($Zn(CH_3COO)_2{\cdot}2H_2O$, Sigma–Aldrich) was mixed with 4.0 g of polyvinyl alcohol solution (18 wt%) (PVA, Sigma–Aldrich, M_w = 30,000–70,000 g/mol) and stirred for 5 h in a water bath at 60 °C. The metal cation concentration of the composite was increased by adding zinc acetate dihydrate, and the PVA/$Zn(CH_3COO)_2$ composites with different $Zn(CH_3COO)_2$ contents ranging from 10 to 20 wt% were obtained. To perform the electrospinning process, the prepared solution was loaded into a plastic syringe and 15 kV potential difference was applied to the tip of a needle of syringe. The distance between the syringe and the metal collector was 6 cm. The feeding rate was kept constant at 4.5 mL/h using a microsyringe pump (LION WZ-50C6). The obtained electrospun fibers were dried under vacuum at 70 °C for 8 h and calcined for 5 h at 500 °C with a heating rate of 4 °C/min in a muffle furnace. Scheme 1 illustrates the procedure of manufacturing electrospun PVA/ZnO composite fibers.

The morphology of ZnO nanofibers was observed under scanning electron microscopy (SEM) using a Philips XL-30S FEG. The diameter of fibers was measured using an image processing software, ImageJ [29]. The crystalline structure of the samples was analyzed using a X-ray diffractometer (Philips X'Pert Pro X-Ray Diffractometer) with Cu Kα radiation.

2.2. Humidity measurements using QCM technique

QCM technique has been used to determine the mass changes due to moist molecules with a resolution of ~1 ng/cm^2. QCM consists of a quartz disk with 0.196 cm^2 area between two Au coated electrodes on both sides. The mass change (Δm) on surface of the quartz crystal was calculated from the frequency change (Δf) as shown by Sauerbrey [30]:

$$\Delta f = -\frac{2f_0^2 \Delta m}{A\sqrt{\mu\rho}} \quad (1)$$

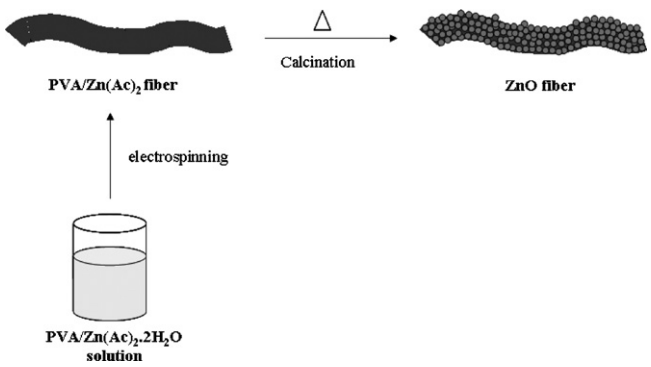

Scheme 1. Schematic representation for preparation of PVA/ZnO composite fibers.

where f_0 is the resonant frequency of the fundamental mode of the QCM crystal, A is the area of the gold coated electrodes on the quartz crystal, ρ is the density, and μ is the shear modulus of quartz substrate. QCM with the model of CHI400A Series from CH Instruments (Austin, USA) has been used to measure the change in the resonance frequency due to mass loading of water molecules after exposure of the QCM electrodes for various humidity levels between 10% and 90% relative humidity (RH). QCM is connected via a USB interface to a computer. QCM electrodes used in our study are made of AT-cut piezoelectric quartz crystal with oscillation frequencies between 7.995 MHz and 7.950 MHz. The density (ρ) of the crystal is 2.684 g/cm^3, and the shear modulus (μ) of quartz is 2.947×10^{11} g/cm s^2. The change of 1 Hz corresponds to the mass of 1.34 ng of materials adsorbed onto the crystal surface of an area of 0.196 cm^2. Both QCM sensor and gold contacts for electrical measurements with 15 μm channel length and 300 μm channel width fabricated with thermal evaporation technique under vacuum of 5×10^{-6} torr.

Scheme 2 shows the experimental setup to investigate the adsorption and desorption kinetics of ZnO nanofiber films under various humidity environments between 10% and 90% RH at room temperature. Relative humidity value inside a test cell with volume of 100 cc is varied between 10% and 90% by controlling the ratio of wet and dry air flow via MKS flow-meter control system between 0 and 1000sccm between 10 steps. The measurements were simultaneously taken using a combined system of QCM sensor and a commercial Sensirion humidity sensor. The sensor has an EI-1050 selectable digital relative humidity and temperature apparatus with a response time of 4 s. The humidity sensor is connected to a PC using a Labview program to collect data via USB port controlled by U12 ADC system combined with a single chip sensor module (SHT11) manufactured by Sensirion (Staefa, Switzerland). The commercial humidity sensor shows 10% RH when 1000sccm of dry air is sent through the QCM cell, while it shows 90% RH when 1000sccm of wet air (obtained by passing dry air through a bubbler kept at a constant temperature of 25 °C).

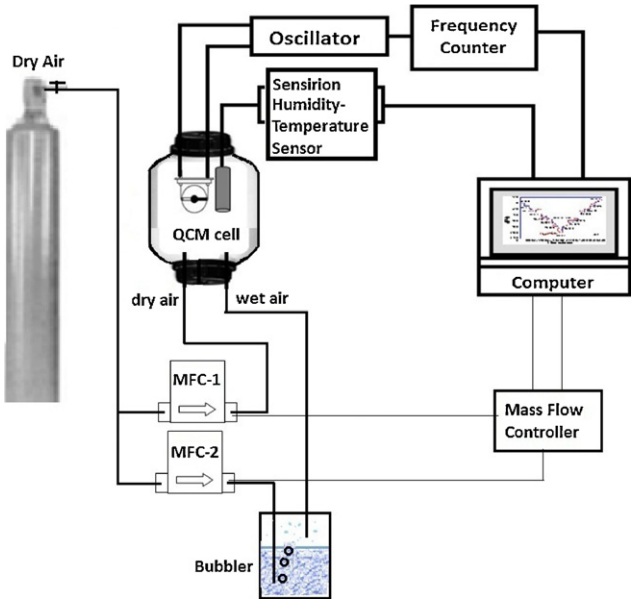

Scheme 2. The experimental QCM setup to measure the adsorption and desorption kinetics of ZnO nanofiber films under various relative humidity conditions between 10% RH and 90% RH.

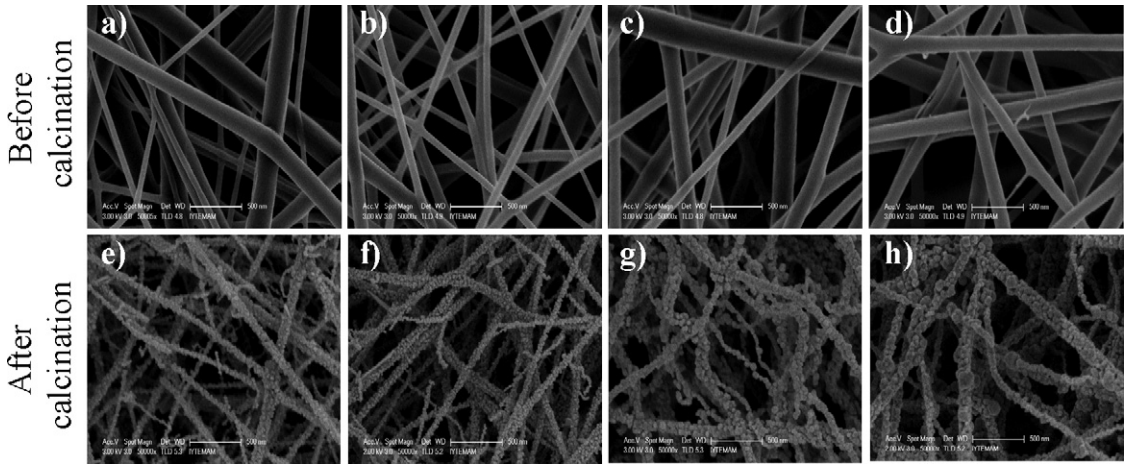

Fig. 1. SEM micrographs of PVA/ZnO composite fibers and ZnO nanofibers with respect to increasing amount of $Zn(Ac)_2{\cdot}2H_2O$ (a, e) 10 wt%, (b, f) 14 wt%, (c, g) 17 wt%, (d, h) 20 wt%.

3. Results and discussion

3.1. Structural characterization of ZnO nanofibers

The graphical demonstration of this entire process is given in Scheme 1. Aqueous solutions of PVA and zinc acetate dihydrate were mixed and homogeneous solutions were electrospun at 2.5 kV cm^{-1}. Fig. 1(a)–(d) shows SEM micrographs of PVA/$Zn(CH_3COO)_2$ fibers (before calcination). They have smooth surface and average fiber diameter (AFD) was in the range of 100–120 nm. The salt content in electrospinning solution is one of the important parameters to control the diameter of fibers. The dependence of the AFD on weight percentage of the salt is shown in Fig. 2. It exhibits an exponential growth with the salt content. The ionic strength of solution is directly proportional with salt concentration. This reflects an increase in current during electrospinning process, *i.e.* solid content transferred from tip to the grounded collector increases. Thus, thicker fibers are obtained in salty electrospinning solutions. The PVA/$Zn(CH_3COO)_2$ fibers were subjected to calcination at 500 °C in air and ZnO-based fibers were obtained. The integrity of fibers remains almost unchanged upon calcination process. However, a significant reduction in diameter was observed approximately 20% on average for all solutions we tried. The occurrence of shrinkage is due to the removal of PVA from the fiber volume and crystallization of ZnO phase (Fig. 1(e)–(h)). In calcination process, the temperature was fixed to 500 °C at which nucleation and growth process readily occurs. Particulate ZnO crystals are evident on the fibers.

XRD pattern of the ZnO fiber mat is displayed in Fig. 3(a). From the diffractogram, eight diffraction planes corresponding to (1 0 0), (0 0 2), (1 0 1), (1 0 2), (1 1 0), (1 0 3), (1 1 2), (2 0 1) are present. They

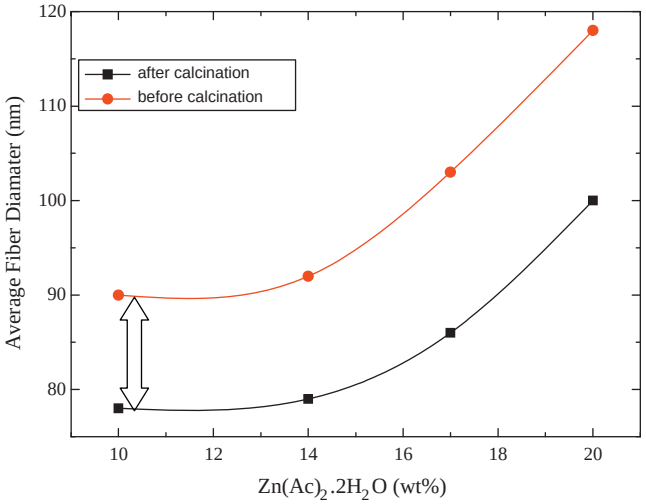

Fig. 2. Average fiber diameter (AFD) versus percent weight of $Zn(Ac)_2{\cdot}2H_2O$.

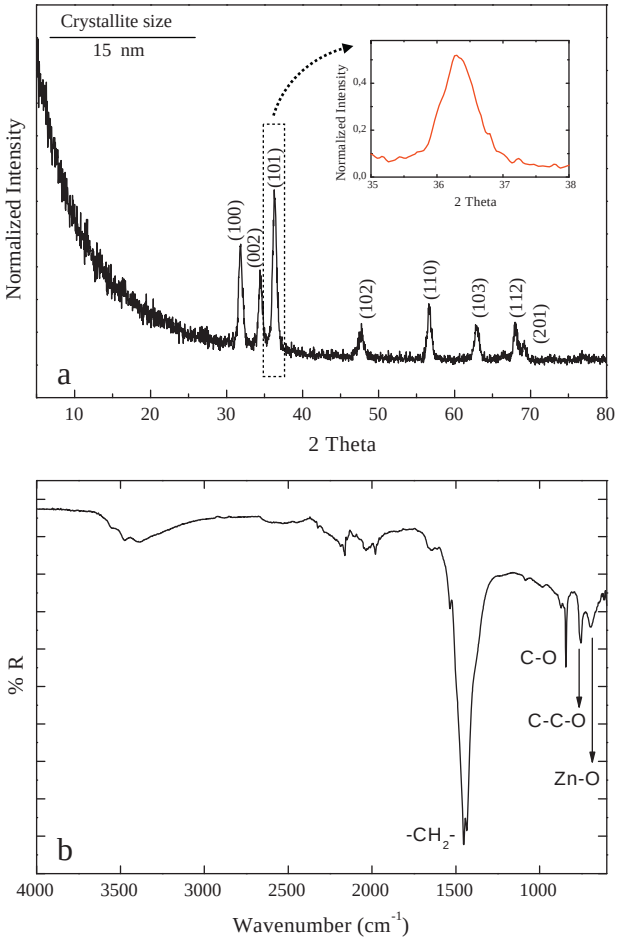

Fig. 3. (a) X-ray diffraction pattern of ZnO nanofibers and the inset is an enlargement of the ZnO (1 0 1) peaks for the calculation of crystallite size. (b) FTIR spectra of ZnO nanofibers after calcination.

are characteristics signals of the wurzite type ZnO phase (JCPDS 79-0207). The average crystallite size of the product was estimated by Debye–Scherrer equation employing on the maximum intense reflection (1 0 1), and it was found to be approximately 15 nm. This size is consistent with the size of particles we observed in SEM micrographs. Fig. 3(b) shows the FTIR spectra of ZnO fibers. Along with the characteristic signal of ZnO at 600 cm^{-1}, an intense signal of $-CH_2$ stretching was also observed at around 1450 cm^{-1}. Moreover, the bands at about 850 and 750 cm^{-1} are assigned to the vibrations of C–O, C–C groups, respectively. The presence of these signals indicates that organic residue still remains in the system and is not removed completely upon calcination. This system was subjected to thermogravimetric analysis to figure out the mass content of organics after calcination process. According to this measurement, approximately 10% organic residue remains in the fibrous system. This amount of polymeric residue may be argued about to reduce the humidity efficiency of material. However, this property meets the requirement of many applications. It must be considered that pure inorganic fibers cannot provide flexibility due to their brittle nature. The presence of low amount of organics in the system may prevent the formation of undesirable brittle nature.

3.2. QCM and electrical responses under varying RH

Fig. 4 shows both adsorptions–desorption responses due to the change in QCM resonance frequency comparing with simultaneously measured resistance changes of ZnO nanofiber coated sensors. The RH lies in the range of 10% and 90%. The negative frequency response (blue line) is given on the left side of the plot, while the corresponding resistance (red circle) is presented on the right side of the plot (For interpretation of the references to color in this text, the reader is referred to the web version of the article.). Three types of adsorption and desorption cycles zoomed out in Fig. 4(b)–(d) have been used to observe reproducibility and sensitivity of ZnO nanofiber coated QCM sensors against the changes in relative humidity. Resistance of the ZnO nanofiber sensor is changed on the order of 4 under 12 V applied bias voltage as a result of the possible disassociation of the adsorbed moist molecules on the oxygen vacancies on the n-type ZnO surface similar to our previous work [7]. Fig. 4(b) shows three cycles of QCM and resistance responses when sent only dry and wet air consequently with 200 s periods to observe maximum adsorption and desorption kinetics. QCM frequency counter is set to '0' Hz as the starting point for the minimum relative humidity at 10% RH when full of dry air with 1000sccm is sent through the test cell. The negative QCM frequency response shows maximum change around – 43 Hz, when wet air with 1000sccm is sent (at 90% RH measured with Sensirion humidity sensor). Resistance of the sensor is decreased from 5×10^{11} to 7×10^{7} Ω. Fig. 4(c) shows the long time (around 1 h) stepwise adsorption and desorption response of ZnO nanofiber loaded QCM and resistive sensors. To create step change in the relative humidity inside the test cell, the wet/dry air ratio is increased to 1000sccm with 200 s intervals. Both QCM frequency response and resistance change showed similar behavior above 60% RH during adsorption/desorption processes. Similar responses are observed when short time relative humidity changes are applied. Fig. 4(d) shows the short time (200 s) adsorption and desorption response of ZnO nanofiber loaded QCM and resistive sensors. To create short time relative humidity pulses, the wet/dry air flow ratio is increased as 100 sccm for each 200 s periods, while after each adsorption process, the maximum desorption process is applied by sending maximum dry air with 1000sccm. The results show that the response time against quick relative humidity changes of ZnO

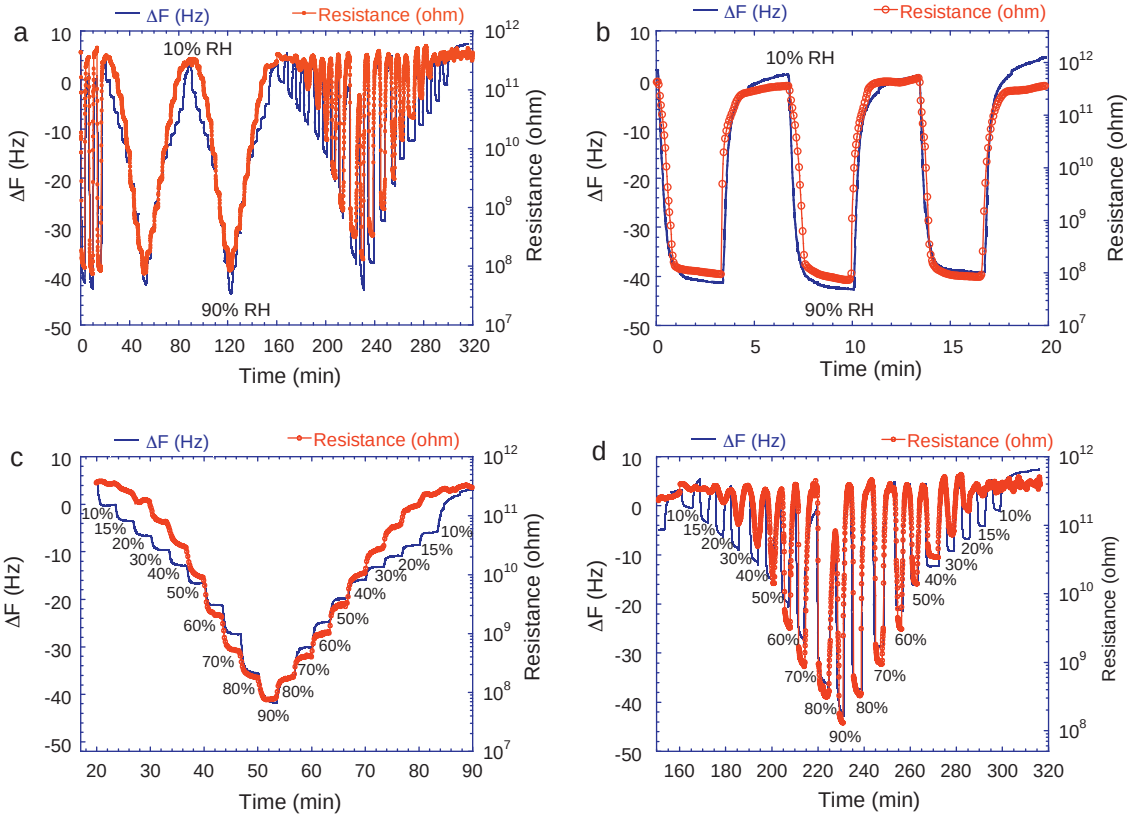

Fig. 4. Adsorption/desorption responses due to QCM resonance frequency changes comparing with simultaneously measured resistance changes of ZnO nanofiber coated sensors between 10% and 90% RH for 6 h (320 min).

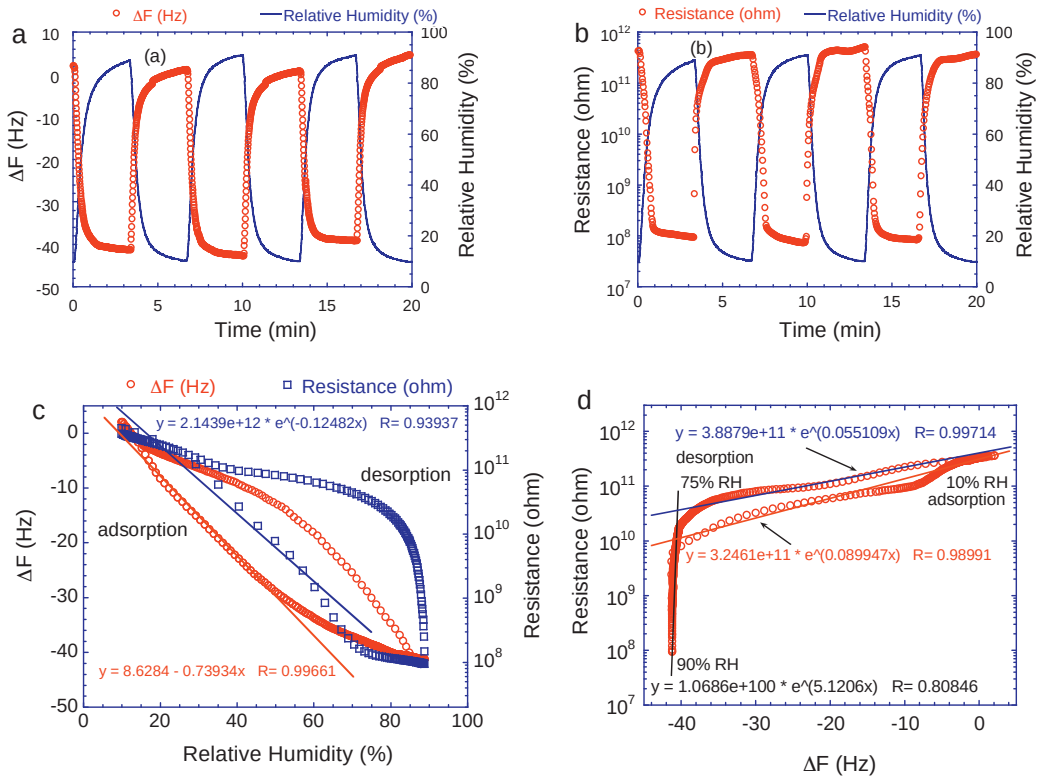

Fig. 5. Adsorption/desorption responses due to QCM resonance frequency (a) and resistance changes (b) of ZnO nanofiber sensors comparing with relative humidity (RH) values simultaneously measured with a Sensirion commercial RH sensor between 10% and 90% RH (c). The exponential relationship between QCM frequency and resistance changes (d).

nanofiber sensors are less than 0.5 s for adsorption process, while it is around 1.5 s, that is, 3 times larger for desorption processes.

Fig. 5 shows maximum adsorption/desorption responses due to QCM resonance frequency and resistance changes of ZnO nanofiber sensors comparing with relative humidity (RH) values simultaneously measured with a Sensirion commercial RH sensor between 10% and 90% RH. There are two distinct behaviors for both QCM and resistance signals before and after 60% RH. The QCM resonance frequency decreases linearly with relatively higher slope ($m = -0.74$RH/Hz) up to 75% RH with increasing relative humidity as shown in Fig. 5(c). Similar trend is observed in resistance changes in Fig. 5(b). But resistance decreases exponentially with increasing relative humidity as shown with exponential fit ($R = 2.14\,e^{-0.125 \times \mathrm{RH}}\ \Omega$).

The hysteresis-like behavior in both QCM and resistance signals between adsorption and desorption process for varying relative humidity between 10% and 90% is clearly seen in Fig. 5(c). But the resistance hysteresis is quite larger during desorption process compare to QCM frequency change. The exponential relationship between QCM frequency and resistance changes is shown in Fig. 5(d). There is a dramatic exponential dependence of resistance change on the amount of absorbed moist molecules during desorption process at higher relative humidity values due to possible condensation. This exponential relationship between adsorbed moist molecules and the increasing conductance of ZnO-based nanofiber sensors under varying relative humidity was explained by Erol et al. with hopping transport mechanism of electrolytic conductance [7]. It is well-known that ZnO is n-type semiconductor due to localized donor levels in the band gap caused by oxygen vacancies and interstitial Zn atoms in the lattice. The oxygen vacancies become active sites for dissociation of the water molecule [31]. The dipoles of the first hydroxylated layer of water meniscus on the surface create an affinity for moisture molecules via van der Waals forces for physisorption process. The electric field applied to the water molecules between gold electrodes with 15 μm gap and under 12 V is close to 0.8×10^6 V/m. Under such a high electric field, hydroxyl groups are formed providing protons as charge carriers of the hopping transport. Hence electrolytic conduction causes an exponential decrease in the resistivity of ZnO nanofiber-based humidity sensor.

The mechanism can also be viewed from macroscopic perspective. Interaction of water molecules with ZnO fiber surface plays an important role in adsorption process. The surface of ZnO fibers is sensitive to atmospheric moisture due to its high reactivity with water molecules. The molecules can be adsorbed on metal oxide surface molecularly either through H bonding or dissociated form of H_2O. Therefore, metal oxide surface is inevitably covered by surface adsorbed water molecules meaning that there is a skin layer made up of surface adsorbed water molecules. The adsorbed water on zinc oxide surface can be categorized into two distinctively different water species: (i) chemisorbed water containing rigid water species with restricted mobility near the solid surface; (ii) physisorbed water molecules that are very loosely adsorbed water molecules which are mobile and can exchange slowly with gaseous water molecules in air [32,33]. Mass transfer of water molecules to and from the interaction region is mainly mediated and facilitated by the latter type of water present on the outermost surface. Demir et al. previously showed the existence of surface-bound water on ZnO using temperature dependence solid state nuclear magnetic (NMR) spectroscopy [34]. Annealing of ZnO nanoparticles at mild temperatures < 360 K were performed during NMR measurement. It was clearly demonstrated that as the annealing process is performed, the proton signal originating from the water species decreases. This result indicates the dynamic desorption process taking place at the physisorbed layer of the watery skin of ZnO nanoparticles. We believe that similar type of

adsorption–desorption process takes place in our particular fibrous ZnO system.

3.3. Theoretical analysis of QCM results using modified Langmuir model

The Langmuir adsorption isotherm model was frequently used to analyze adsorption data to explain the adsorption–desorption kinetics of gas molecules in the literature [7,35]. Basically, the relationship between the surface adsorption and desorption rates and frequency shift (Δf) for QCM can be expressed as follows:

$$\frac{d\Delta f}{dt} = (\Delta f_{\max} - \Delta f)k_a C - k_d \Delta f \quad (2)$$

where $\Delta f_{\max}$ is the maximum frequency change at the maximum humidity range, C is the concentration of the adsorbed gas, k_a and k_d are the adsorption and desorption rates, respectively. Integration of Eq. (2) leads to the solution of the first order differential equation as follows:

$$\Delta f(t) = \Delta f_{\max} K'(1 - e^{-k_{obs}t}) \quad (3)$$

where K' is the association constant and k_{obs} is the inverse of the relaxation time. The change in the mass due to moisture adsorption can be fitted to the Langmuir adsorption isotherm model since the frequency shift is directly proportional with the change of the absorbed mass according to the Sauerbrey relation given in Eq. (1). The time dependence of the amount of absorbed water molecules on the film surface Δm_t can be defined as,

$$\Delta m_t = \Delta m_\infty (1 - e^{-t/\tau}) \quad (4)$$

where $\tau^{-1} = k_a[\text{water vapour molecules}] + k_d$ is the maximum adsorbed mass of the moist molecules on the surface, for very long times, when $t \to \infty$, is calculated as 54.75 ng.

Fig. 6 shows the least square fit (solid line) using the Langmuir adsorption isotherm model given in Eq. (4) for the adsorption parts of the data between 10% RH and 84% RH given in Fig. 5(b). The relaxation time τ is obtained as 0.3 min. The average values of adsorption (k_a) and desorption rates (k_d) between 10% RH and 90% RH were calculated as 3453.6 M^{-1} s^{-1} and 0.0147s^{-1}, respectively.

The corresponding Gibbs free energy ΔG of adsorption/desorption process at a constant temperature can be calculated with $\Delta G = -RT \ln K_{eq}$ [36], where K_{eq} is equilibrium constant ($K_{eq} = k_a/k_d$), R is the universal gas constant and T is the temperature (298 K). The calculated equilibrium constant K_{eq} and Gibbs free energy values are 234,939 and −30.64 kJ/mol for the adsorbed water mass between 10% and 90% RH, respectively. The Gibbs free energy with negative sign shows that there is an energy loss for water molecules on ZnO nanofiber film surface during adsorption process.

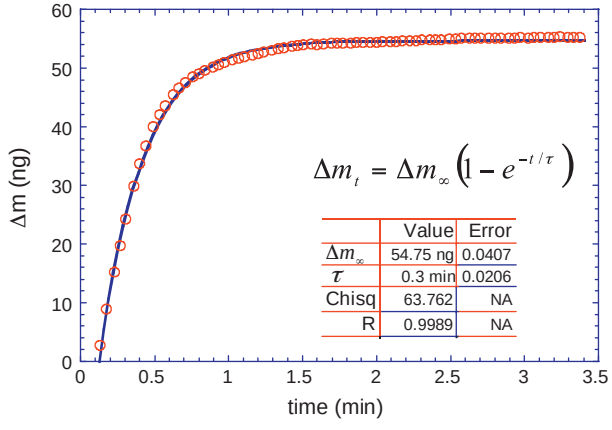

Fig. 6. The least square fit (solid line) to the Langmuir adsorption isotherm model given in Eq. (4) for the adsorbed water mass between 10% and 84% RH.

4. Conclusion

In this study, Quartz Crystal Microbalance (QCM) technique is used to analyze the water vapor adsorption and desorption kinetics of ZnO-based fiber mats obtained by electrospinning. The resistance of the fiber sensor decreases by about four orders of magnitude with increasing relative humidity (RH) from 10% to 90% RH. The response and recovery time of the sensor are around 0.5 s and 1.5 s, respectively. The QCM resonance frequency decreases linearly while the resistance decreases exponentially with the increasing RH. The adsorption and desorption of moisture rates and Gibbs free energy kinetic parameters were determined by using dynamic Langmuir model. The values of adsorption and desorption rates were calculated as 3453.6 M^{-1} s^{-1} and 0.0147s^{-1}, respectively. The Gibbs free energy for adsorption cycle is found to be as −30.64 kJ/mol. Thus, QCM results show that the ZnO nanofiber mats are very sensitive to relative humidity changes and give reproducible adsorption and desorption kinetic behaviors for both short and long time periods. The mats on QCM respond like a commercial RH sensor and can be used for potential humidity sensor applications.

Acknowledgements

This project was partially supported by IYTE Scientific Research Project with project number 2008IYTE31 and Tubitak (Turkish Scientific Association) under project number TBAG 109T240. The authors acknowledge The Center of Material Research at IYTE for assistance in microscopy imaging. S.O. thanks to Nesli Yağmurcukkardes for helping during humidity measurements.

Appendix A. Supplementary data

Supplementary data associated with this article can be found, in the online version, at doi:10.1016/j.talanta.2011.05.031.

References

[1] M. Pelino, C. Cantalini, M. Faccio, Act. Passive Electron. Compon. 16 (1994) 69–87.
[2] Y. Zhang, K. Yu, D. Jiang, Z. Zhu, H. Geng, L. Luo, Appl. Surf. Sci. 242 (2005) 212–217.
[3] S. Okur, N. Uzar, N. Tekgüzel, A. Erol, M.Ç. Arıkan, Physica E (Amsterdam, Neth.), in press, doi:10.1016/j.physe.2010.08.015.
[4] F.-T. Liu, S.-F. Gao, S.-K. Pei, S.-C. Tseng, C.-H.J. Liu, J. Taiwan Inst. Chem. Eng. 40 (2009) 528–532.
[5] J.-A. Park, J. Moon, S.-J. Lee, S.H. Kim, H.Y. Chu, T. Zyung, Sens. Actuators B 145 (2010) 592–595.
[6] Q. Qi, T. Zhang, Q. Yu, R. Wang, Y. Zeng, L. Liu, H. Yang, Sens. Actuators B 133 (2008) 638–643.
[7] A. Erol, S. Okur, B. Comba, Ö. Mermer, M.Ç. Arıkan, Sens. Actuators B 145 (2010) 174–180.
[8] Y. Qiu, S. Yang, Adv. Funct. Mater. 17 (2007) 1345–1352.
[9] H. Zhang, Z. Li, W. Wang, C. Wang, J. Am. Ceram. Soc. 93 (2010) 142–146.
[10] Q. Qi, T. Zhang, S. Wang, X. Zheng, Sens. Actuators B 137 (2009) 649–655.
[11] W. Wang, Z. Li, L. Liu, H. Zhang, W. Zheng, Y. Wang, H. Huang, Z. Wang, C. Wang, Sens. Actuators B 141 (2009) 404–409.
[12] W. Wang, H. Huang, Z. Li, H. Zhang, Y. Wang, W. Zheng, C. Wang, J. Am. Ceram. Soc. 91 (2008) 3817–3819.
[13] J.-A. Park, J. Moon, S.-J. Lee, S.-C. Lim, T. Zyung, Curr. Appl. Phys. 9 (2009) S210–S212.
[14] B. Ding, M. Wang, J. Yu, G. Sun, Sensors 9 (2009) 1609–1624.
[15] H. Wu, D. Lin, R. Zhang, W. Pan, J. Am. Ceram. Soc. 91 (2008) 656–659.
[16] J.-J. Wu, S.-C. Liu, Adv. Mater. 14 (2002) 215–218.
[17] B. Liu, H.C. Zeng, J. Am. Chem. Soc. 125 (2003) 4430–4431.
[18] H. Xia, Y. Wang, F. Kong, S. Wang, B. Zhu, X. Guo, J. Zhang, Y. Wang, S. Wu, Sens. Actuators B 134 (2008) 133–139.
[19] B.C. Yadav, R. Srivastava, C.D. Dwivedi, P. Pramanik, Sens. Actuators B 131 (2008) 216–222.
[20] B.C. Yadav, R. Srivastava, C.D. Dwivedi, P. Pramanik, Sens. Actuators A 153 (2009) 137–141.

[21] M.M. Demir, I. Yilgor, E. Yilgor, B. Erman, Polymer 43 (2002) 3303–3309.
[22] M.M. Demir, M.A. Gülgün, Y.Z. Menceloglu, B. Erman, S.S. Abramchuk, E.E. Makhaeva, A.R. Khokhlov, V.G. Matveeva, M.G. Sulman, Macromolecules 37 (2004) 1787–1792.
[23] M.M. Demir, G. Uğur, M.A. Gülgün, Y.Z. Menceloğlu, Macromol. Chem. Phys. 209 (2008) 508–515.
[24] R. Ramaseshan, S. Sundarrajan, R. Jose, J. Appl. Phys. 102 (2007) 111101.
[25] Ü. Özgür, Y.I. Alivov, C. Liu, A. Teke, M.A. Reshchikov, S. Doğan, V. Avrutin, S.-J. Cho, H. Morkoç, J. Appl. Phys. 98 (2005) 041301.
[26] S. Hess, M.M. Demir, V. Yakutkin, S. Baluvhev, G. Wegner, Macromol. Rapid Commun. 30 (2009) 394–401.
[27] B. Ding, M. Wang, X. Wang, J. Yu, G. Sun, Mater. Today 13 (2010) 16–27.
[28] X. Hu, J. Gong, L. Zhang, J.C. Yu, Adv. Mater. 20 (2008) 4845–4850.
[29] Public domain software to be downloaded from National Institute of Health. http://rsb.info.nih.gov/ij.
[30] G. Sauerbrey, Z. Phys. 155 (1959) 206.
[31] R. Schaub, P. Thostrup, N. Lopez, E. Lægsgaard, I. Stensgaard, J.K. Nørskov, F. Besenbacher, Phys. Rev. Lett. 87 (2001) 266104–266111.
[32] M. Nagao, J. Phys. Chem. 76 (1971) 3822–3828.
[33] M.M. Demir, K. Koynov, Ü. Akbey, I. Lieberwirth, G. Wegner, Macromolecules 40 (2007) 1089–1100.
[34] M.M. Demir, P. Castignolle, Ü. Akbey, G. Wegner, Macromolecules 40 (2007) 4190–4198.
[35] S. Okur, M. Kuş, F. Özel, V. Aybek, M. Yılmaz, Talanta 81 (2010) 248–251.
[36] S. Qiu, L. Sun, H. Chu, Y. Zou, F. Xu, N. Matsuda, Thin Solid Films 517 (2009) 2905–2911.